Influence of the Quantum Capacitance on Electrolyte Conductivity through Carbon Nanotubes

Théo Hennequin-Nespoulous, Manoel Manghi, Adrien Noury, Francois Henn, Vincent Jourdain, John Palmeri

Quantum capacitance governs electrolyte conductivity in carbon nanotubes

Théo Hennequin and Manoel Manghi*
Laboratoire de Physique Théorique, Université Paul Sabatier–Toulouse III, CNRS, France

Adrien Noury, François Henn, Vincent Jourdain, and John Palmeri†
Laboratoire Charles Coulomb, Université de Montpellier, CNRS, France
(Dated: July 25, 2023)

In recent experiments, unprecedentedly large values for the conductivity of electrolytes through carbon nanotubes (CNTs) have been measured, possibly owing to flow slip and a high pore surface charge density whose origin is still unknown. By accounting for the coupling between the *quantum* CNT and the *classical* electrolyte-filled pore capacitances, we study the case where a gate voltage is applied to the CNT. The computed surface charge and conductivity dependence on reservoir salt concentration and gate voltage are intimately connected to the CNT electronic density of states. This approach provides key insight into why metallic CNTs have larger conductivities than semiconducting ones.

Although much experimental, theoretical, and molecular modeling effort has been devoted over the past years to understanding water and ion (electrolyte) transport through carbon nanotubes (CNTs) [1–3], the origin of the electric charge localized on the surface of industrially important CNT based nanofluidic systems still remains unclear (see Ref. [4] and references therein). It has already been proposed that this surface charge could arise from functional groups at the CNT entrances [5, 6] and/or the specific adsorption of ions, such as OH^- [7]. Although the above cited studies lead to the conclusion that this surface charge plays a key role in governing ion transport in CNTs, it is difficult to regulate it directly and one is left to making inferences, for example by studying the variation of ionic conductance G with the pH or salt concentration, c_s, of the external bulk reservoirs bounding the CNT. Intriguing results have been obtained, including a power law behavior, $G \propto c_s^\alpha$, with $1/2 \leq \alpha \leq 1$, which could be interpreted as the manifestation of an underlying surface charge regulation mechanism [8–10].

Through a simplified feasibility study we propose in this work that by biasing a CNT incorporated in a nanofluidic system *via* an applied gate voltage, V_g, and taking into account explicitly the quantum capacitance (QC) of the quasi-1D CNT structure as well as the non-linear capacitance of the confined electrolyte ion the pore, it should be possible to quantify the CNT surface charge density $\sigma_{\rm Q}$ and establish a link between the intrinsic CNT electronic properties and ion transport through the same structure, such as the electrolyte conductance through the CNT. A major conclusion it that these intrinsic electronic properties will depend significantly, under certain conditions, on whether the CNT is metallic (M) or semiconducting (SC).

The CNT quantum charge $\sigma_{\rm Q}$ arises from the low density of states (DOS) for the charge carriers (electrons and holes) in this quasi-1D system. Indeed, the applied V_g creates a net charge on the CNT by perturbing the equilibrium occupation of the allowed energy levels. Part of V_g goes to raising the electric potential of the CNT to ψ_0 and part goes to shifting the chemical potential by $\Delta\mu = -eV_{\rm ch} = -e(V_g - \psi_0)$ (where e is the absolute value of the electron charge): ψ_0 will then be lower than V_g with (in the absence of other capacitances) the difference between the two giving rise to the chemical contribution, $V_{\rm ch}$. The amplitude of the chemical potential shift is determined by V_g and the relative values of the capacitances with the smallest one providing the most important contribution. We show here that for a wide range of salt concentration, $10^{-3} \leq c_s \leq 4$ mol/L, the CNT QC, $C_{\rm Q}$, can be lower than the nanopore electrolyte contribution, $C_{\rm P}$, and therefore the quantum contribution controls the conductance. By comparing the confined electrolyte conductivity calculated for a classical metallic nanopore (with a very high, effectively infinite, DOS) [11] with those calculated for M and SC CNTs, we bring to light clear signatures of each type of CNT behavior.

The CNT QC has already been studied in setups where an electrolyte surrounds the CNT and acts as an electrolyte liquid gate, the main goal was however to investigate the electrical properties of the CNT itself [12–17]. Within this context, Lemay's group [12–14] has carried out an interesting study, although the capacitance of the external electrolyte was modeled using an overly simplified form (of the type used for Stern layers) that does not capture the full complexity of the non-linear capacitance of an electrolyte. The QC of graphene sheets and ribbons have also been studied theoretically and experimentally using both ionic liquid and electrolyte gates [14, 18, 19]. The gating of a generic nanopore has also been studied theoretically for confined electrolytes in a nanofluidic setup where the gate voltage is applied to an electrode in contact with an insulating layer making up the finite-thickness surface of a nanopore [20, 21]. The confined electrolyte conductance was investigated, but the important special case of a CNT was not addressed: the system was treated as being purely classical and therefore the capacitances considered were the geometrical one coming

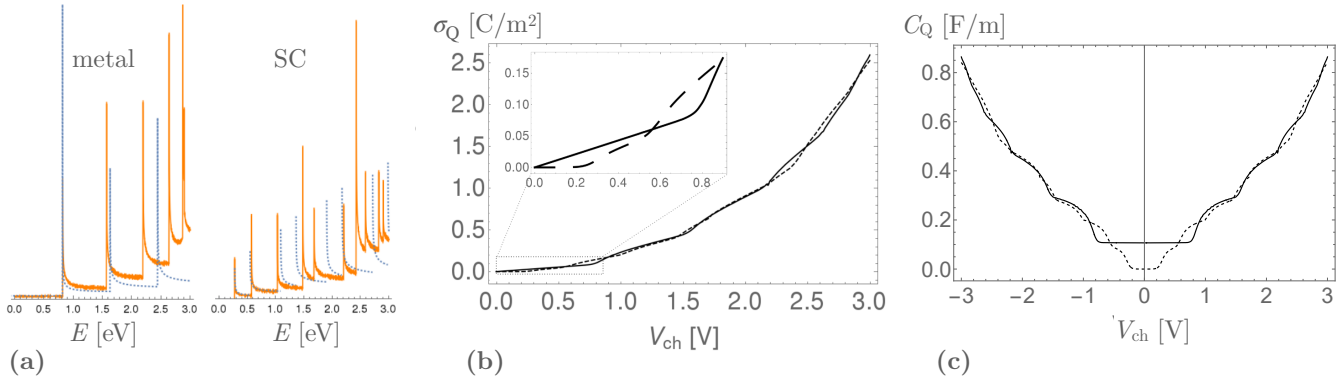

Figure 1. (a) Density of states (DOS) $g(E)$ for metallic (M,left) and semi-conducting (SC,right) CNTs computed by the tight-binding method (solid orange lines) and the $\mathbf{k}\cdot\mathbf{p}$ approximation (blue dashed lines). (b) Quantum surface charge density and (c) integral QCs vs. the chemical contribution, $V_{\rm ch}$ for these M (solid curve) and SC (dotted curve) CNTs.

from the insulating layer, together with the Stern and non-linear Graham capacitances of the electrolyte.

In contrast to these previous studies we show here that by examining the confined electrolyte conductivity the CNT QC can provide a direct adjustable handle on the all important, but elusive, nanopore surface charge density. By shedding light in a fundamental way on ion transport in this type of nanofluidic system, it should be possible to pave the way to the tuning of transport properties for particular practical applications.

We briefly summarize the electronic characteristics of single-walled carbon nanotubes (SWCNTs) obtained by simplified theoretical methods and tight-binding calculations (see Ref. [23] for more details). A SWCNT can be considered as a graphene sheet rolled up into a cylinder and its electronic nature, metallic (M) or semiconducting (SC), depends on its atomic structural characteristics fixed by two *chiral* indices (n,m) that determine its diameter and chirality [12, 22–24]. The simplified theoretical $\mathbf{k}\cdot\mathbf{p}$ method, which neglects curvature effects, reveals that in the M case, $|n-m|=3q$, where $q\in\mathbb{N}$. In the SC case, $|n-m|\neq 3q$ and the size of the band gap is inversely proportional to the SWCNT diameter d [**?**]. The band structure is composed of multiple 1D subbands sliced from the Dirac dispersion cone of graphene and, as shown by simplified theoretical analyses [22], exhibits a certain amount of (approximate) universality. The ith electron-hole subband has the following dispersion relation

$$E_{\pm}(i,k)=\pm\sqrt{(\hbar v_F k)^2+E_i^2}, \qquad (1)$$

where $v_F\approx 8\times10^5$ m/s is the Fermi velocity at the Dirac cone, $\hbar$ the reduced Planck's constant, k the charge carrier wave vector, and $E_i=2\hbar v_F i/(3d)$. The allowed values of i depend on whether the SWCNT is M or SC [22, 25]. The $E_{i,g}=2E_i$ are the individual energy gaps determined by the distance of the quantized k states from the center of the Dirac cone situated where both k and E vanish. The DOS per unit surface (the usual DOS per unit length divided by πd), for a SC SWCNT is given by [12, 22–24]

$$g_{\rm SC}(E)=g_0\sum_{i>0,\neq 3q}\frac{|E|}{\sqrt{E^2-E_i^2}}\Theta(|E|-E_i), \qquad (2)$$

where $g_0=4/(\pi^2 d\hbar v_F)$ and Θ is the Heaviside unit step function. The SC band gap is predicted to be $E_g=E_+(1,0)-E_-(1,0)=2E_1=0.7/d$ eV, if d is in nm (between 0.2 to 0.7 eV for $1\leq d\leq 3$ nm). For purposes of illustration we choose here $d=1.5$ nm for which $E_g=0.47$ eV (18 k_BT at room temperature). The subbands for $i=3q$ (integer q) are not present [see Fig. 1(a)] and therefore the SC DOS exhibits van Hove singularities at $|E|=E_i$ for $i>0, i\neq 3q$.

For true M SWCNTs, $E_g=0$ and the first band has a non-zero DOS $g(0)=g_0$ and a half-width equal to E_3 as shown in Fig. 1(a)] [23]. The $\mathbf{k}\cdot\mathbf{p}$ method leads to a DOS given by [22]

$$g_{\rm M}(E)=g_0+2g_0\sum_{m>0}\frac{|E|}{\sqrt{E^2-(mE_3)^2}}\Theta(|E|-mE_3). \qquad (3)$$

The M DOS exhibits van Hove singularities at $|E|=mE_3$ for $m>0$ and, aside from the conduction band, all bands are doubly degenerate.

We show in Fig. 1(a) the approximate theoretical DOS for $d=1.5$ nm (dashed blue curves) and the DOS computed by the group of Maruyama [26] using the tight-binding method (solid orange curves) for a M CNT of chiral indices $(11,11)$ ($d=1.512$ nm) and for a SC CNT of chiral indices $(19;0)$ ($d=1.508$ nm). It is clear that the approximate DOS universality breaks down for $|E|>1$ eV where the actual DOS begins to depend on the values of the chiral indices.

At thermal equilibrium without external perturbations the chemical potential is situated at the Dirac point taken as the reference $\mu = 0$ eV. When a gate voltage V_g is applied to an electrode posed on a CNT, a shift in the chemical potential, $\Delta\mu$, occurs and the occupation of the allowed levels is modified, which leads to the creation of charges (electrons or holes) in the various subbands labeled by i. The CNT DOS plays a crucial role in determining the amplitude of this charge. The density of electrons (number per unit surface), n, for a SWCNT is calculated as a function of temperature T and $\Delta\mu$ using Fermi statistics [12, 22–24],

$$n(\Delta\mu) = \int_{E_g/2}^{\infty} \frac{g(E)}{1+\exp[\beta(E-\Delta\mu)]} dE, \qquad (4)$$

where $\beta = 1/(k_B T)$ ($k_B T \approx 25$ meV at room temperature). The density of holes, p, is given by Eq. (4) by replacing $-\Delta\mu$ by $\Delta\mu$. The *chemical contribution* to the applied gate voltage (electromotive force), $V_{\rm ch} = V_g - \psi_0$ engenders a charge per unit surface,

$$\sigma_{\rm Q}(V_{\rm ch}) = e(p-n), \qquad (5)$$

and is related to the chemical potential shift through $\Delta\mu = -eV_{\rm ch}$, where ψ_0 is the electrostatic potential drop between the CNT and the reference electrode. Note that $\sigma_{\rm Q} = 0$ for $V_{\rm ch} = 0$, $\sigma_{\rm Q} > 0$ for $V_{\rm ch} > 0$, and $\sigma_{\rm Q} < 0$ for $V_{\rm ch} < 0$ [27, 28]. The surface charge densities $\sigma_{\rm Q}(V_{\rm ch})$ for SC and M CNTs are plotted in Fig. 1(b). For $V_{\rm ch} > 1$ V, they almost superimpose, showing some slope discontinuities associated with the van Hove singularities of the associated DOS. As seen in the inset, however, for $V_{\rm ch} < 1$ V the two are quite different, essentially because the charge density vanishes in the gap for the SC CNT, i.e. for $V_{\rm ch} < E_g/(2e) = 0.23$ V.

We distinguish between the *integral* QC needed here,

$$C_{\rm Q} \equiv \frac{|\sigma_{\rm Q}|}{V_{\rm ch}}, \qquad (6)$$

which directly determines the charge on the CNT, and the *differential* one, $C_Q^d(V_{\rm ch}) \equiv \partial|\sigma_{\rm Q}|/\partial V_{\rm ch}$, which gives access directly to many features of the DOS. The integral capacitances for SC and M CNTs are plotted in Fig. 1(c). If $|V_{\rm ch}| < E_3/e$ holds, then $C_{\rm Q} \simeq C_Q^0$ for M CNTs and $C_{\rm Q} = 0$ for SC ones. For larger $|V_{\rm ch}|$, similarly to $\sigma(V_{\rm ch})$, the two integral capacitances are quite similar.

In the simplified description we adopt here (absence of any residual geometrical capacitance arising from the rest of the electrical circuit) the gate voltage, $V_g = V_{\rm ch} + \psi_0$, is shared between the chemical contribution and the electrostatic one. The equivalent electrical circuit is shown in Fig. 2(a), the total capacitance, $C_{\rm tot}$, and amplitudes of each contribution to V_g depend on the individual capacitances and are given by [12, 19, 27, 28]:

$$\frac{1}{C_{\rm tot}} = \frac{1}{C_{\rm Q}} + \frac{1}{C_{\rm P}} = \frac{V_g}{|\sigma_{\rm Q}|}, \qquad (7)$$

where $C_{\rm P} = |\sigma_{\rm Q}|/\psi_0$ is the non-linear integral *pore* capacitance arising from electrolyte confined to the interior of a CNT, which leads to:

$$\psi_0 = V_g \frac{C_{\rm Q}(V_{\rm ch})}{C_{\rm Q}(V_{\rm ch}) + C_{\rm P}(\psi_0)}. \qquad (8)$$

This result shows clearly that if $C_{\rm Q} \gg C_{\rm P}$ then $\psi_0 \lesssim V_g$ and $V_{\rm ch} \ll V_g$, indicating that quantum effects are negligible. It corresponds to the "classical" limit. Conversely, if $C_{\rm P} \gg C_{\rm Q}$, then $\psi_0 \ll V_g$ and quantum effects are dominant.

To calculate the electrolyte capacitance, $C_{\rm P}$, we use an interpolation formula for the electric potential at the pore wall, ψ_0, that we previously devised for small nanopores [10]. This formula for ψ_0 as a function of the nanopore radius R ($= d/2$), electrolyte salt concentration c_s, and nanopore surface charge density, $\sigma_{\rm P}$, becomes exact in the good coion exclusion and homogeneous limits and is an accurate interpolation elsewhere:

$$\sinh\tilde{\psi}_0 = \frac{\sigma_{\rm P}^*(1+\sigma_{\rm P}^*)}{\tilde{c}_s}, \qquad (9)$$

where $\tilde{\psi}_0 = \beta e|\psi_0|$ and

$$\tilde{c}_s = \pi \ell_B R^2 c_s, \qquad \sigma_{\rm P}^* = \frac{\pi R \ell_B}{e}|\sigma_{\rm P}| \qquad (10)$$

are respectively the dimensionless electrolyte salt concentration and surface charge density (the electric potential at the reference electrode in the bulk reservoir is taken to be zero). The Bjerrum length is $\ell_B = e^2/(4\pi\epsilon k_B T) \simeq 0.7$ nm in bulk water at room temperature (dielectric permittivity $\epsilon = 78\epsilon_0$). Eq. (9) can be rewritten by isolating $\sigma_{\rm P}^*$ as

$$\sigma_{\rm P}^* = \frac{1}{2}\left(\sqrt{1+4\tilde{c}_s \sinh\tilde{\psi}_0} - 1\right). \qquad (11)$$

For a classical metal (effectively infinite DOS), formally $C_{\rm Q}/C_{\rm P} \to \infty$ and using Eq. (8) we see that the surface charge density $\sigma_{\rm cl}^*$ is given by Eq. (11) with ψ_0 set to V_g. In this case for low enough $\tilde{c}_s$ and V_g, $\sigma_{\rm cl}^* \simeq \tilde{c}_s \sinh(\beta e V_g)$ and for high enough $\tilde{c}_s$ and $V_g \gg 25$ mV, $\sigma_{\rm cl}^* \simeq \tilde{c}_s^{1/2} e^{\beta e V_g/2}$. The rapid exponential rise in surface charge density in the latter limit appears to be compatible with the extremely high conductivities observed in [11] for gold plated nanopores at negative gate voltages (for which specific ion adsorption can be neglected). Given the low DOS of CNTs we do not expect such classical exponential behavior for them. In this case by keeping $\sigma_{\rm P}^*$ constant, $\tilde{\psi}_0$ is low when $\tilde{c}_s$ is high, which increases the pore capacitance and eventually leads to $C_{\rm P} \gg C_{\rm Q}$, i.e. quantum effects become important.

By defining $C_{\rm P} = \frac{4\epsilon}{R}\tilde{C}_{\rm P}$, the integral pore capacitance can be found from the dimensionless one:

$$\tilde{C}_{\rm P} = \frac{\sigma_{\rm P}^*}{\tilde{\psi}_0} = \frac{\sqrt{1+4\tilde{c}_s \sinh\tilde{\psi}_0} - 1}{2\tilde{\psi}_0} \qquad (12)$$

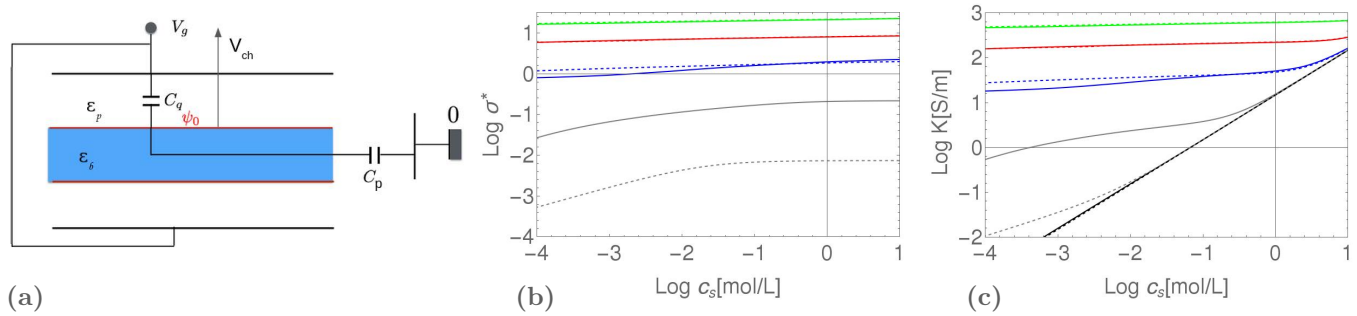

Figure 2. (a) Equivalent electrical circuit of the system with the quantum capacitance C_Q and the pore one C_P. The gate voltage, $V_g = \psi_0 + V_{ch}$, is divided between the potential at the inner CNT surface, ψ_0, and the chemical contribution, V_{ch}. (b) Dimensionless surface charge density σ^* and (c) conductivity of a KCl electrolyte vs. salt concentration c_s (Log-Log plot) for the M (solid lines) and SC (dashed lines) CNTs with $V_g = 0.2$ (grey), 1 (blue), 2 (red), and 3 V (green). The thick line is the bulk conductivity.

For $\tilde{\psi}_0 \ll 1$, $\tilde{C}_P \to \tilde{c}_s$ and $C_P \to \epsilon R/(2\lambda_{DH}^2)$, where $\lambda_{DH} = (8\pi\ell_B c_s)^{-1/2}$ is the bulk Debye-Hückel screening length for a monovalent electrolyte. In this limit the electrolyte filled pore acts as a parallel plate capacitor of capacitance ϵ/d_{eff} with effective thickness $d_{eff} = 2\lambda_{DH}^2/R$.

Now by writing $\sigma \equiv \sigma_Q = \sigma_P$ and combining $\sigma_Q(V_g - \psi_0)$ from Eq. (5) and Eq. (9), we obtain $\tilde{c}_s(V_g, \psi_0)$, which enables us to trace a parametric plot of σ as a function of c_s for fixed gate voltage V_g by varying ψ_0 from 0 to V_g. This is shown in Fig. 2(b) for the SC and M cases for $V_g = 0.2, 1, 2$ and 3 V. For $V_g = 0.2$ V, the surface charge density is two orders of magnitude larger for the M CNT than for the SC one. This is because V_g is just below $E_g/2$ (gap half-width). At this relatively low value of V_g the surface charge density increases quickly with c_s at low concentrations. For higher gate voltages, σ increases very slowly with c_s, being almost constant for $V_g \geq 2$ V. For $V_g = 1$ V (blue curves) $\sigma(\text{SC}) > \sigma(\text{M})$ at low c_s because ψ_0 is high and V_{ch} is too low to reach beyond the SC van Hove singularity occurring at $E_g/(2e) = 0.23$ V [see Fig. 1(a)]. For large c_s, however, ψ_0 becomes lower and $V_{ch} \simeq E_3/e = 0.7$ V higher, now reaching the large first van Hove singularity for the M case.

The pore conductance G is related to the conductivity κ through $G = \pi R^2 \kappa/L$ where L is the pore length. The pore conductivity, κ, as a function of σ^* and $\tilde{c}_s$ can be obtained using the result obtained in Eq. 19 of Ref. [10], which takes into account the electrical migration contribution (first two terms) and the electro-osmotic one (third term), including flow slip at the pore surface:

$$\tilde{\kappa} = (\tilde{\mu}_+ + \tilde{\mu}_-)\tilde{c}_s\sqrt{1 + \left(\frac{\sigma^*}{\tilde{c}_s}\right)^2} - \text{sgn}(\sigma)\sigma^*(\tilde{\mu}_+ - \tilde{\mu}_-) + 2\sigma^*\left[1 - \frac{\ln(1+\sigma^*)}{\sigma^*} + 2\tilde{b}\sigma^*\right], \quad (13)$$

where $\tilde{\kappa} = (2\pi^2 R^2 \ell_B^2 \eta\kappa/e^2)$ is the dimensionless conductivity ($\eta = 8.94 \times 10^{-4}$ Pa.s being the water viscosity), $\tilde{\mu}_\pm = 2\pi\eta\ell_B\mu_\pm$ the dimensionless mobilities of ions (taken equal to the bulk values, $\mu_+ \approx \mu_- = 5 \times 10^{-11}$ s/kg for KCl), and $\tilde{b} = b/R$ is the ratio between the slip length b and the pore radius [sgn(σ) denotes the sign of σ]. In Eq. (13) the conductivity $\kappa(c_s, V_g)$ is a function of both c_s and V_g because $\sigma(c_s, V_g)$ is a function of both these quantities.

One observes in Fig. 2(c), that the conductivity is enhanced compared to the bulk case for intermediate and low salt concentrations. This is the signature of a non-zero surface charge density. For $V_g > 1$ V, this enhancement even persists to high c_s, attesting to a high surface charge density. At low salt concentration, κ in Eq. (13) is controlled by σ (good coion exclusion regime) and we therefore observe in Fig. 2(c) an increase in conductivity similar to the one observed for $\sigma(c_s)$. We have checked that for $V_g > 1$ V, $\sigma^* > \tilde{c}_s$ over the whole concentration range and κ is therefore controlled by the first electrical migration term in Eq. (13), which is one order of magnitude larger than the electro-osmotic one (the second term is negligible since $\mu_+ \approx \mu_-$ for KCl). For the M case and $V_g < 1$ V (solid grey line), κ increases with c_s, but much more slowly than the bulk one, with an apparent exponent smaller than 1/2.

By taking a slip length large enough, the electro-osmotic contribution in Eq. (13) associated with the fluid slip at the nanopore surface, $4\tilde{b}\sigma^{*2}$, can eventually dominate the electrical migration one. For instance, if a reasonable value of $\tilde{b} = 40$ [29] is taken, the electro-osmotic contribution is greater by one order of magnitude over the whole concentration range. The conductivity would then be completely controlled by $\sigma^*(c_s)$ [plotted in Fig. 2(b)], as a more complete study (underway) will reveal.

Changing the concentration in micrometric reservoirs is not easy in practice. One could measure more easily the electrolyte conductivity at fixed c_s by varying V_g. To present the conductivity in this way, we first compute ψ_0 by solving numerically $\sigma_Q(V_g - \psi_0) = \sigma_P(c_s, \psi_0)$ using

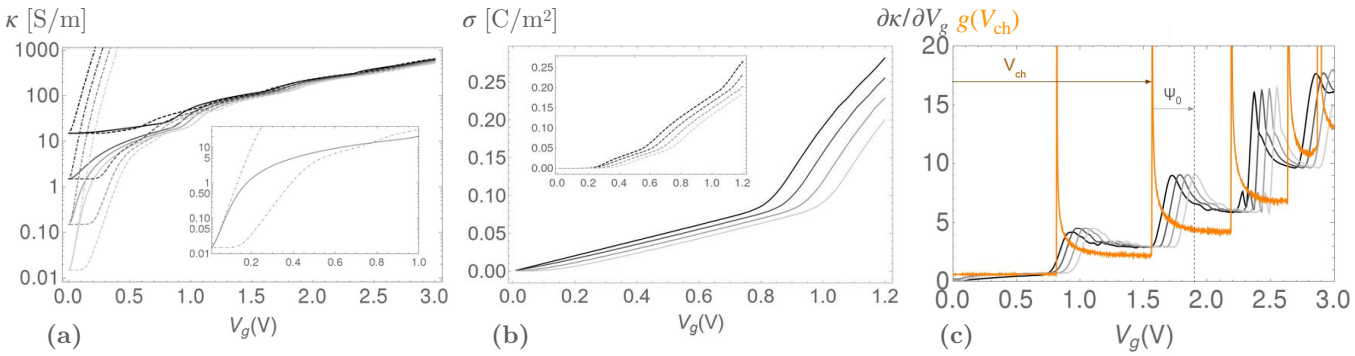

Figure 3. (a) Electrolyte conductivity κ vs. gate voltage V_g in M (solid lines) and SC (dashed lines) CNTs for reservoir salt concentration values of (from bottom to top) $c_s = 10^{-3}, 10^{-2}, 10^{-1}, 1$ mol/L. The classical metallic CNT is shown in dotted-dashed lines. The inset is a zoom for $c_s = 10^{-3}$ mol/L. (b) Associated surface charge density vs. V_g for the M CNT for the same c_s values as in (a). The SC CNT is shown in the inset. (c) Derivative of the electrolyte conductivity, $\kappa'(V_g)$, in the M CNT for the same c_s values as in (a). The DOS $g(V_{\rm ch})$ is superimposed in orange. To illustrate how to read off ψ_0 we show it and $V_{\rm ch}$ for the case $c_s = 10^{-3}$ mol/L and $V_g = 1.9$ V.

Eqs. (5) and (11) at fixed V_g and c_s. We then re-inject ψ_0 in $\sigma_{\rm P}$, which itself can finally be injected into Eq. (13). In Fig. 3(a) we plot the conductivity as a function of V_g at fixed $c_s = 10^{-3}, 10^{-2}, 10^{-1}, 1$ mol/L from bottom to top. We confirm that κ varies strongly at low gate voltages. For $V_g = 0$, $\sigma = 0$ and $\kappa \propto c_s$ (bulk conductivity), which explains the staggered values (separated by a decade) at low V_g. The distinction between the three cases, semiconductor, quantum metal and "classical" metal is clear at low V_g, where the QC suppresses the "classical" exponential growth of conductivity with V_g for M and SC CNTs and the SC energy gap suppresses the conductivity with respect to that of the quantum metal. The M CNT conductivity follows the classical one at very low V_g within a window the decreases in width with increasing c_s. At high V_g all M and SC curves are almost superimposed.

Even if the quantum surface charge density σ, has the same derivative as the classical one at $V_g = 0$, it becomes quickly linear $\sigma \simeq C_{\rm Q}^0 V_g$, with a lower slope up to $V_g \simeq E_3/e \simeq 0.7$ V, as shown in Figure 3(b). Indeed, for not too low V_g, $C_{\rm Q} \ll C_{\rm P}$, which implies that $C_{\rm tot} \simeq C_{\rm Q} \approx C_{\rm Q}^0$ and therefore $\psi_0 \ll V_g$. We have checked that this is true whenever $C_{\rm P}/C_{\rm Q}^0 \gg 1$, which leads to $\sqrt{\tilde{c}_s} > \tilde{C}_{\rm Q}^0$. Since $\tilde{C}_{\rm Q}^0 = 0.03$, this last inequality is verified for $\tilde{c}_s > 10^{-3}$ [the case for the concentrations shown in Fig. 3(a)]. For lower reservoir salt concentrations, σ is no longer linear in V_g. These different behaviors are illustrated in the inset of Fig. 3(a) where we also note the impact of the SC CNT gap, which leads to a constant κ up to $V_g = 0.2 \simeq E_g/e$ V, the edge of the gap. We conclude that the QC has a considerable effect on both σ and κ as soon as $V_g > k_B T/e \approx 25$ mV and this over the whole experimental range of c_s.

The structure of a conductivity curve $\kappa(V_g)$ exhibiting slope changes, related to the DOS structure, is easier to visualize by plotting its derivative $\kappa'(V_g)$ [see Fig. 3(c)] and superimposing on it the DOS $g(V_{\rm ch})$ (in orange). Clearly the peaks in $\kappa'(V_g)$ are directly connected to the van Hove singularities of the DOS with an offset to the right which increases when c_s decreases. Indeed, since κ is governed by the surface charge density $\sigma_{\rm Q}$ which depends only on $V_{\rm ch} = V_g - \psi_0$, the higher ψ_0 is (and therefore the lower c_s is), the more $\kappa(V_g - \psi_0)$ is shifted to the right. We can therefore directly measure the potential ψ_0 in Fig. 3(c). For instance, for $c_s = 10^{-3}$ mol/L and $V_g = 1.9$ V, we get $\psi_0 \simeq 0.32$ V. This is a way to readily check that for these c_s values, $\psi_0 \ll V_g$, thus confirming the central role played by the QC on the conductivity.

As an concluding example, we consider the experimental results obtained by Liu et al. [30], who measured, for $c_s = 1$ mol/L, conductances of 61.0 nS for M SWCNTs and 5.6 nS for SC ones with $0.8 \leq d \leq 2$ nm and $5 \leq L \leq 10$ nm. Using the DOS given in Fig. 1(a) with $d = 1.5$ nm and $L = 8$ nm, we can account for these two conductance values by taking $V_g \simeq 0.35$ V, a value that we interpret as an environmentally induced shift in the zero of the gate tension.

More systematic experiments are clearly needed to ascertain to what extent the charge density and therefore the electrolyte conductivity through SWCNTs can be controlled by an applied gate voltage. Presumably, a more complete model for conductivity would be needed to account for the full complexity of real CNTs, including the influence of pH (via charge regulation), residual geometrical capacitances, and dielectric interactions.

* manoel.manghi@univ-tlse3.fr
† john.palmeri@umontpellier.fr

[1] S. Guo, E. R. Meshot, T.Tevye Kuykendall, S. Cabrini, and F. Fornasiero, Nanofluidic Transport through Isolated Carbon Nanotube Channels: Advances, Controversies, and Challenges, Adv. Mater., **27**, 5726-5737 (2015).

[2] J. P. Thiruraman, P. M. Das, and M. Drndic, Ions and Water Dancing through Atom-Scale Holes: A Perspective toward "Size Zero", ACSNano, **14**, 3736-3746 (2020).

[3] N. R. Aluru *et al.*, Fluids and Electrolytes under Confinement in Single-Digit Nanopores, Chem. Rev. 2023, **123**, 2737-2831 (2023).

[4] M. Manghi, J. Palmeri, F. Henn, A. Noury, F. Picaud, G. Herlem, and V. Jourdain, Ionic Conductance of Carbon Nanotubes: Confronting Literature Data with Nanofluidic Theory, J. Phys. Chem. C, **125**, 22943-22950 (2021).

[5] S. Balme, F. Picaud, M. Manghi, J. Palmeri, M. Bechelany, S. Cabello-Aguilar, A. Abou-Chaaya, P. Miele, E. Balanzat, J.-M. Janot, Ionic transport through sub-10 nm diameter hydrophobic high-aspect ratio nanopores: experiment, theory and simulation, Sc. Rep. **5**, 10135 (2015).

[6] K. Yazda, S. Tahir, T. Michel, B. Loubet, M. Manghi, J. Bentin, F. Picaud, J. Palmeri, F. Henn, and V. Jourdain, Voltage-activated transport of ions through single-walled carbon nanotubes, Nanoscale **9**, 11976 (2017).

[7] B. Grosjean, C. Pean, A. Siria, L. Bocquet, R. Vuilleumier, and M.-L. Bocquet, Chemisorption of hydroxide on 2D materials from DFT calculations: graphene versus hexagonal boron nitride, J. Phys. Chem. Lett., **7**, 4695-4700 (2016).

[8] E. Secchi, A. Nigues, L. Jubin, A. Siria, L. Bocquet, Scaling Behavior for Ionic Transport and its Fluctuations in Individual Carbon Nanotubes, Phys. Rev. Lett., **116**, 154501 (2016).

[9] P. M. Biesheuvel and M. Z. Bazant, Analysis of ionic conductance of carbon nanotubes, Phys. Rev. E, **94**, 050601(R) (2016).

[10] M. Manghi, J. Palmeri, K. Yazda, F. Henn and V. Jourdain, Role of charge regulation and flow slip in the ionic conductance of nanopores: An analytical approach, Phys. Rev. E, **98** 012606 (2018).

[11] P. Gao and C. R. Martin, Voltage Charging Enhances Ionic Conductivity in Gold Nanotube Membranes, ACSNano, **8**, 8266-8272 (2014).

[12] I. Heller, J. Kong, K.A. Williams, C. Dekker, and S. G. Lemay, Electrochemistry at Single-Walled Carbon Nanotubes: The Role of Band Structure and Quantum Capacitance, J. Am. Chem. Soc., **128** 7353-7359 (2006).

[13] I. Heller, A. M. Janssens, J. Mannik, E. D. Minot, S. G. Lemay, and C. Dekker, Identifying the Mechanism of Biosensing with Carbon Nanotube Transistors, Nano Lett., **8** 591-595 (2008).

[14] I. Heller, S. Chatoor, J. Mannik, M. A. G. Zevenbergen, C. Dekker, and S. G. Lemay, Influence of Electrolyte Composition on Liquid-Gated Carbon Nanotube and Graphene Transistors, J. Am. Chem. Soc. **131** 17149-17156 (2010).

[15] S. Rosenblatt, Y. Yaish, J. Park, J. Gore, V. Sazonova, and P. L. McEuen, High Performance Electrolyte Gated Carbon Nanotube Transistors, Nano Lett., **2**, 869-872 (2002).

[16] J. Li, P. H. Q. Pham, W. Zhou, T. D. Pham, and P. J. Burke, Carbon-Nanotube-Electrolyte Interface: Quantum and Electric Double Layer Capacitance, ACSNano, **12**, 9763-9774 (2018).

[17] J. Li, and P. J. Burke, Measurement of the combined quantum and electrochemical capacitance of a carbon nanotube, Nature Comm., **10**, 3598 (2019).

[18] J. Xia, F. Chen, J. Li and N. Tao, Measurement of the quantum capacitance of graphene, Nature Nanotech., **4**, 505-509 (2009).

[19] T. Fang, A.Konar, H.Xing, and D. Jena, Carrier statistics and quantum capacitance of graphene sheets and ribbons, Appl. Phys. Lett. **91** 092109 (2007).

[20] Z. Jiang and D. Stein, Electrofluidic Gating of a Chemically Reactive Surface, Langmuir, **28** 8161 (2010).

[21] Z. Jiang and D. Stein, Charge regulation in nanopore ionic field-effect transistors, Phys. Rev. E, **83** 031203 (2011).

[22] J.W. Mintmire and C.T. White, Universal Density of States for Carbon Nanotubes, Phys. Rev. Lett., **81** 2506 (1998).

[23] M.J. Biercuk, S. Ilani, C.M. Marcus, and P.L. McEuen, In Carbon Nanotubes, Eds. A. Jorio, G. Dresselhaus, M.S. Dresselhaus, Electrical Transport in Single-Wall Carbon Nanotubes, Topics Appl. Physics **111**, 455 (2008).

[24] S. Ilani, L. A. K. Donev, M. Kindermann, and P. L. McEuen, Measurement of the quantum capacitance of interacting electrons in carbon nanotubes, Nature Phys., **2**, 687-691 (2006).

[25] T. Miyake and S. Saito, Quasiparticle band structure of carbon nanotubes, Phys. Rev. B, **68**, 155424 (2003).

[26] S. Maruyama web page, The University of Tokyo: `http://photon.t.u-tokyo.ac.jp/~maruyama/kataura/1D_DOS.html`

[27] H. Zhang, C. Berthod, H. Berger, T. Giamarchi, A. F. Morpurgo, Band Filling and Cross Quantum Capacitance in Ion-Gated Semiconducting Transition Metal Dichalcogenide Monolayers, Nano Lett., **19**, 8836 (2019).

[28] C. Berthod, H. Zhang, A. F. Morpurgo, and T. Giamarchi, Theory of cross quantum capacitance, Phys. Rev. Res., **2**, 043036 (2021).

[29] S. K. Kannam, P. J. Daivis, and B. Todd, Modeling slip and flow enhancement of water in carbon nanotubes, MRS Bull., **42**, 283-288 (2017).

[30] L. Liu, C. Yang, K. Zhao, J. Li, and H.-C. Wu, Ultrashort single-walled carbon nanotubes in a lipid bilayer as a new nanopore sensor, Nature Comm., **4**, 2989 (2013).